Supporting Information for

Photochemical aging of atmospheric fine particles as a potential source for gas-phase hydrogen peroxide

Pengfei Liu, Can Ye, Chenglong Zhang, Guangzhi He, Chaoyang Xue, Junfeng Liu, Chengtang Liu, Yuanyuan Zhang, Yifei Song, Xuran Li, Xinming Wang, Jianmin Chen, Hong He, Hartmut Herrmann, Yujing Mu*
Email: yjmu@rcees.ac.cn

This file includes:
Supplementary text
Figures S1 to S13
Table S1
SI References

Supplementary text

S1. Winter field campaign.

Measurements of atmospheric H_2O_2, NO, $PM_{2.5}$ and RH were performed from 4 November to 31 December 2017 at the Station of Rural Environment, Research Center for Eco-Environmental Sciences (SRE-RCEES, 38.7° N, 115.3° E) in Wangdu, Baoding, Hebei Province of the North China Plain (NCP). Detailed information about the rural site was given in our previous studies [1, 2]. H_2O_2 was measured by a commercial H_2O_2 monitor based on wet chemical dual enzyme fluorescence detection by Lazarus et al. [3] (Model AL-2021, AERO-laser, Germany). NO was detected by a chemiluminescence instrument (Model 42i, Thermo, USA). $PM_{2.5}$ mass concentrations were measured by a standard Tapered Element Oscillating Microbalance system (Model TEOM 1405A, Thermo, USA). Atmospheric RH was monitored by a portable weather station (Model WXT520, Vaisala, Finland).

S2. Chemical and optical analysis.

One quarter of each micro-quartz fiber filter sample was extracted ultrasonically with 20 mL ultrapure water for half an hour. After being purified through a syringe-driven filter (MillexGV PVDF, 0.22 μm; Millipore, Ireland), the solutions were used for measuring water-soluble ions (WSIs; SO_4^{2-}, NO_3^-, Cl^-, Na^+, NH_4^+, Mg^{2+}, Ca^{2+} and K^+), water-soluble organic carbon (WSOC) and light absorption spectra (200-900 nm) of water-soluble components (WSCs) by an ion chromatograph (IC6200, Wayeal, China), a total carbon analyzer (TOC-L, Shimadzu, Japan) and an UV-vis spectrophotometer (DR6000, HACH, USA), respectively. Then, the light absorption capability, also named as mass absorption efficiency (MAE, $m^2\ g^{-1}$), was calculated by the following expression, which represents the water-soluble light absorbance per unit mass of $PM_{2.5}$ [4, 5]:

$$MAE_{\lambda} = (Abs_{\lambda} - Abs_{700}) \times \frac{V_s}{L \times M} \times \ln(10)$$

where Abs_{λ} is the light absorption at λ nm; V_s is the volume (mL) of extraction solutions; L is the path length (cm) of light; M is the mass (μg) of $PM_{2.5}$. The light absorption at 700 nm (Abs_{700}) was obtained from the average value between 695 nm and 705 nm to avoid the possible errors due to the baseline drift [6].

Another quarter of each sample was digested with 8 mL of mixed aqueous solutions of HCl (6 mL) and HNO_3 (2 mL) by a microwave reaction system (Multiwave PRO, Anton Paar, Germany). The metal elements (MEs; Al, Mn, Fe, Ba, Ni, Cu, Zn, As, Se and Pb) were analyzed by an inductively coupled plasma-mass spectrometer (ICP-MS, Agilent 8800, USA). The rest of each micro-quartz fiber filter sample was cut into a circular area of 0.5 cm^2 for the measurements of organic carbon (OC) and element carbon (EC) by a thermal/optical carbon analyzer (DRI-2001A, USA) with the IMPROVE thermal/optical reflectance protocol. Detailed measurement information has been described in the previous studies [1, 6-9]. The concentrations of the chemical components (WSIs, WSOC, MEs, OC and EC) from the $PM_{2.5}$ samples were displayed in Table S1. Based on the USEPA TO-11A method (USEPA, 1999), atmospheric carbonyls (formaldehyde, acetaldehyde, acetone and propionaldehyde) were collected into 2, 4-dinitrophenylhydrazine (DNPH)-coated silica gel cartridges (Sep-Pak, Waters, USA) at the outlet of the flow tube with a flow rate of 1.2L min^{-1} for 1 h before and after irradiation, respectively. After sampling, the cartridges were eluted immediately by 5 mL acetonitrile and analyzed by a high-performance liquid chromatograph (HPLC, Wayeal, China) with acetonitrile-water binary mobile phase [10-13].

S3. Density functional theory (DFT) calculations.

Spin-polarized density functional theory (DFT) calculations with periodic boundary conditions (PBC) were performed using the Perdew-Burke-Ernzerhof (PBE) functional

[14] as implemented in the Vienna *ab initio* simulation package (VASP 5.4.4) [15]. The projector augmented wave method (PAW) was used to describe the core-valence electron interaction [16]. The plane wave energy cutoff was set to 400 eV for all atoms. A graphene plane with a rectangular boundary (17.04×17.22 $Å^2$) was used as the model of carbonaceous soot surfaces [17, 18]. A vacuum spacing of 20 Å was used to avoid the periodic image interaction normal to the surface. The supercells were sufficiently large to use only Γ point sampling for integration over the Brillouin zone [17]. The conjugate gradient algorithm was used for geometry optimization until the forces on all atoms were less than 0.02 eV/Å. The Gaussian smearing method with a smearing width of 0.2 eV was applied to accelerate the convergence of integration at the Brillouin zone. The reaction pathways and transition states were traced by the climbing image nudged elastic band (CI-NEB) method with a spring constant of 5.0 eV/$Å^2$ [19-21]. Frequency analysis was performed to confirm the transition states and their connected minima.

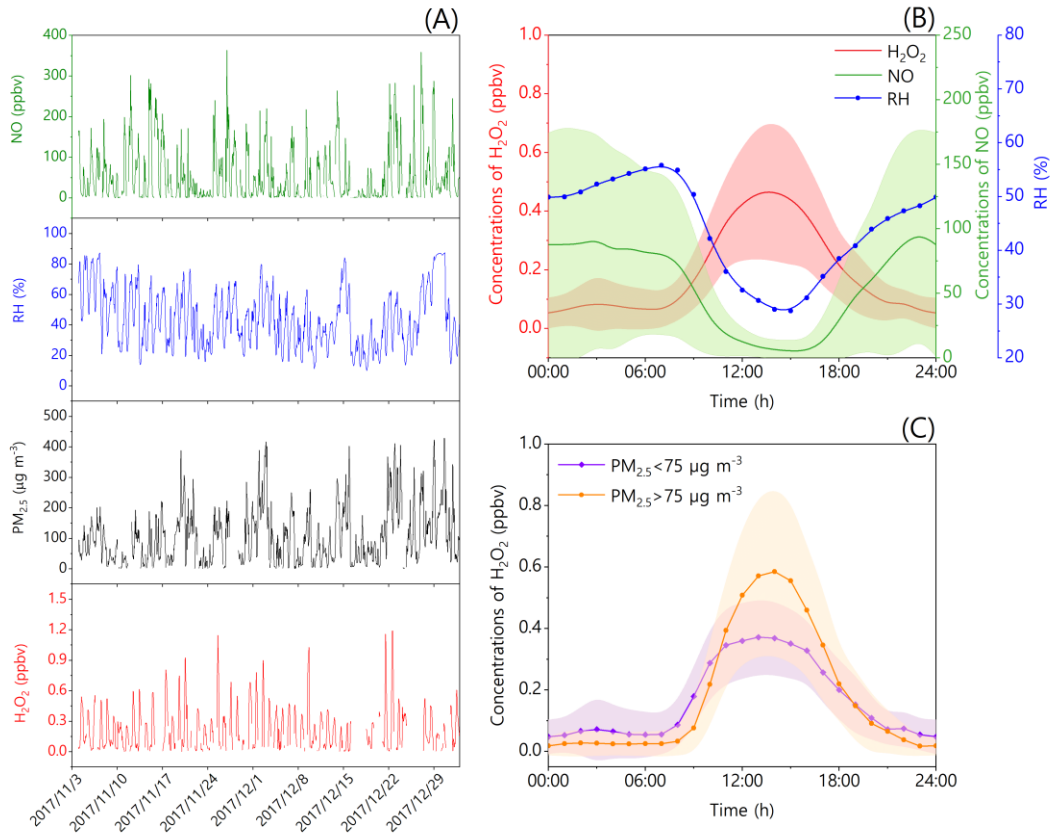

Fig. S1. Time series of NO, RH, $PM_{2.5}$ and H_2O_2 (A), diurnal variations of H_2O_2, NO and RH (B), and diurnal variations of H_2O_2 under low (<75 μg m^{-3}) and high (>75 μg m^{-3}) $PM_{2.5}$ conditions (C) during the winter field campaign in the North China Plain.

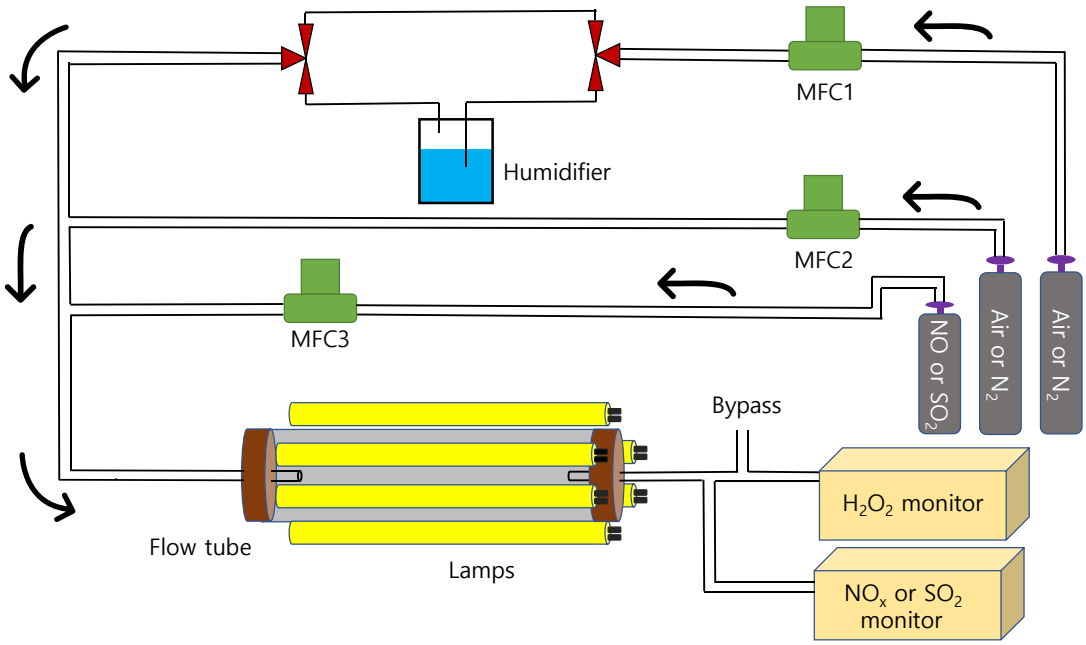

Fig. S2. Sketch of the photochemical flow tube reactor setup.

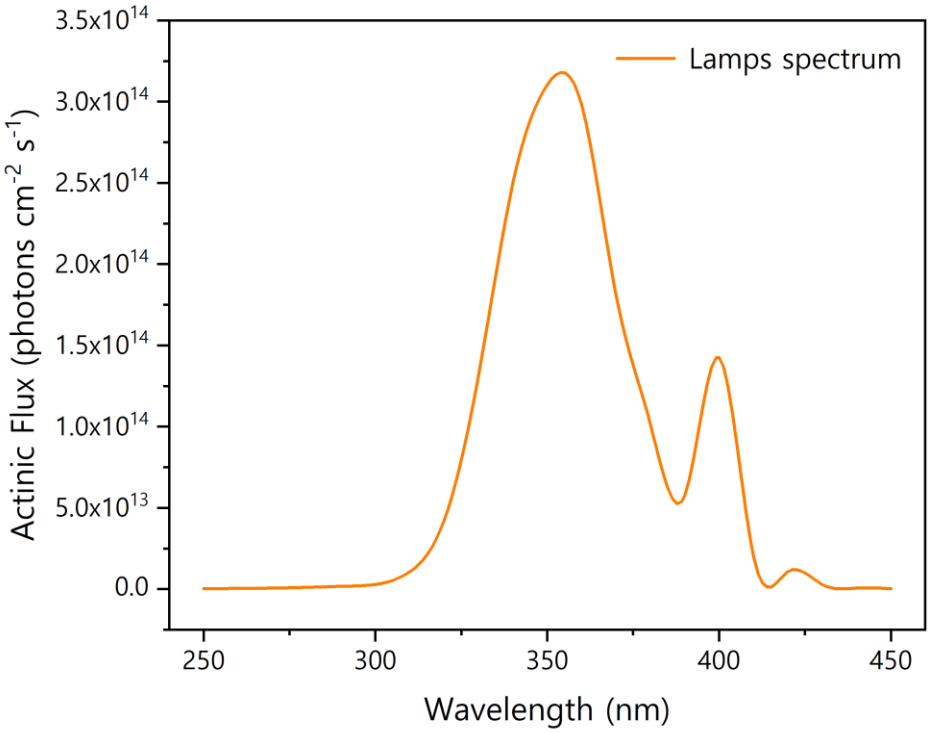

Fig. S3. Irradiance spectrum of the fluorescent lamps used in the flow tube.

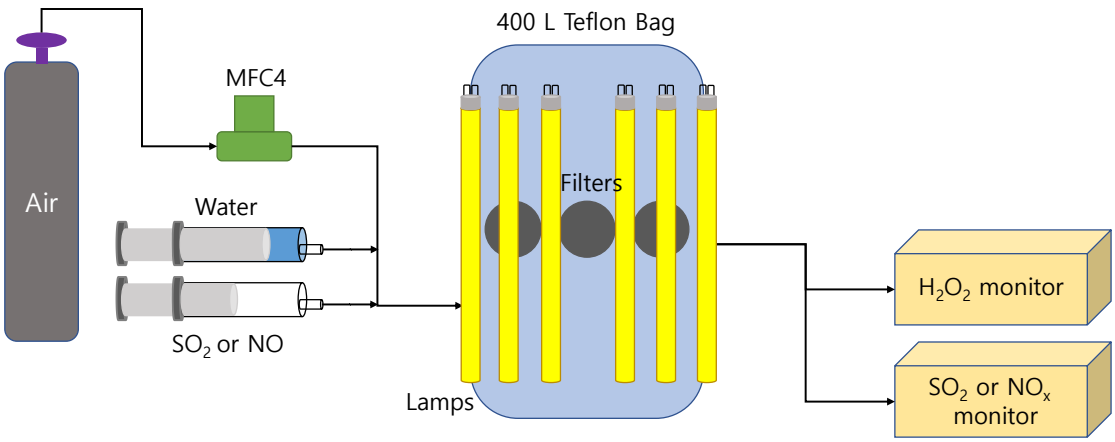

Fig. S4. Sketch of the photochemical smog chamber reactor setup.

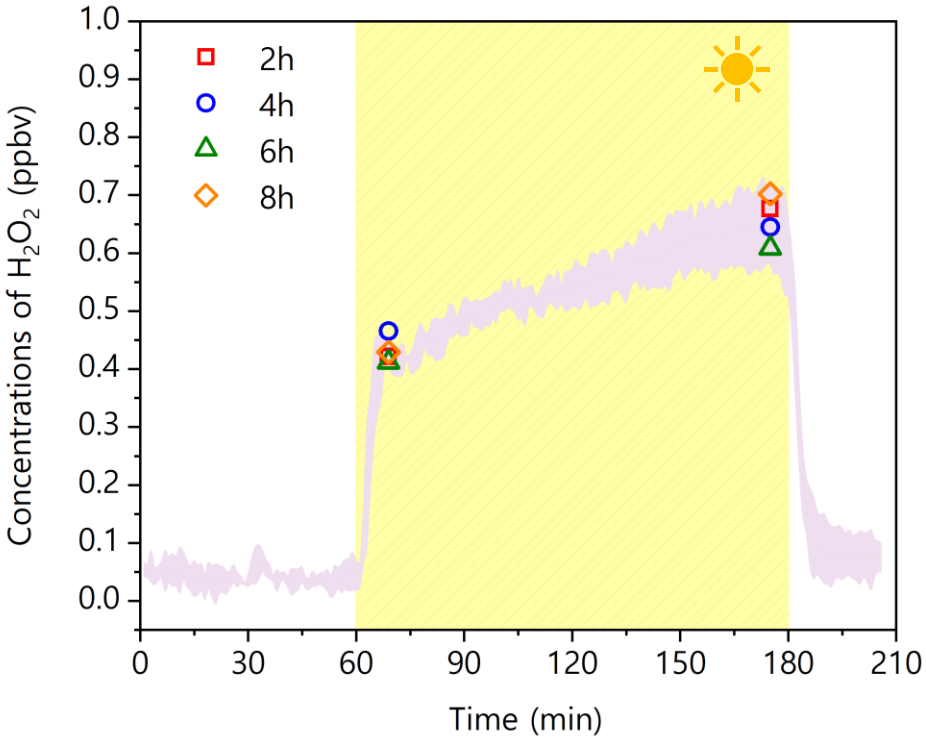

Fig. S5. The influence of $PM_{2.5}$ loadings on H_2O_2 production from $PM_{2.5}$ filter samples under irradiation of the UV lamps in the flow tube. The experiments were carried out for the $PM_{2.5}$ filter samples (WD-16-Apr-20) collected during 2h, 4h, 6h and 8h by flushing humidified synthesis air of ~15% RH (296 ± 2K) at a flow rate of 5L min^{-1}. The blank areas and the yellow shadows represent the dark condition and the UV irradiation, respectively.

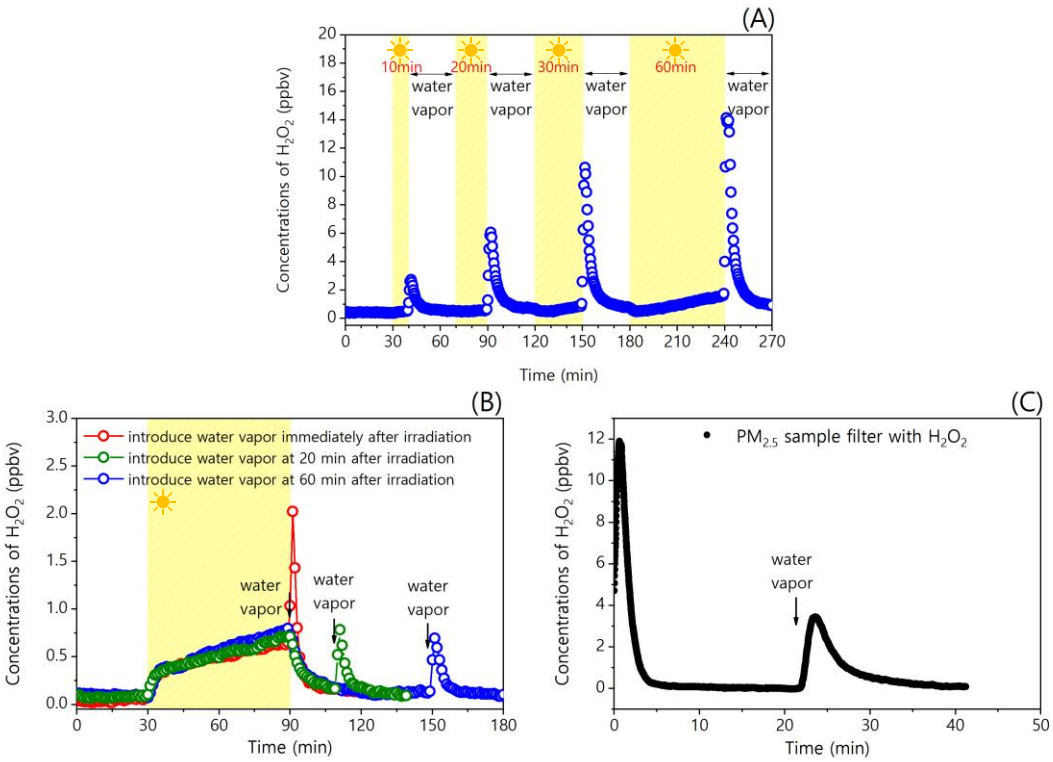

Fig. S6. The influence of water vapor on H_2O_2 production from $PM_{2.5}$ filter samples under irradiation of the UV lamps in the flow tube. The blank areas, the yellow shadows and the black arrows represent the dark condition, the UV irradiation, and the introduction of water vapor (~15% RH), respectively. All experiments were conducted at room temperature (296 ± 2 K) with flushing synthesis air at a flow rate of 5L min^{-1}. **(A)** The experiment was carried out for the $PM_{2.5}$ filter sample (WD-18-Jan-19) under 10 min, 20 min, 30 min and 60 min irradiation, respectively, before introducing water vapor. **(B)** The experiments were carried out for the same $PM_{2.5}$ filter sample (WD-10-Jan-20) by introducing water vapor at 0 min, 20 min and 60 min intervals, respectively, after irradiation. **(C)** The experiment was carried out for the $PM_{2.5}$ filter sample (WD-2-Jan-20) preloaded with a certain fraction of H_2O_2 until equilibrium condition before introducing water vapor.

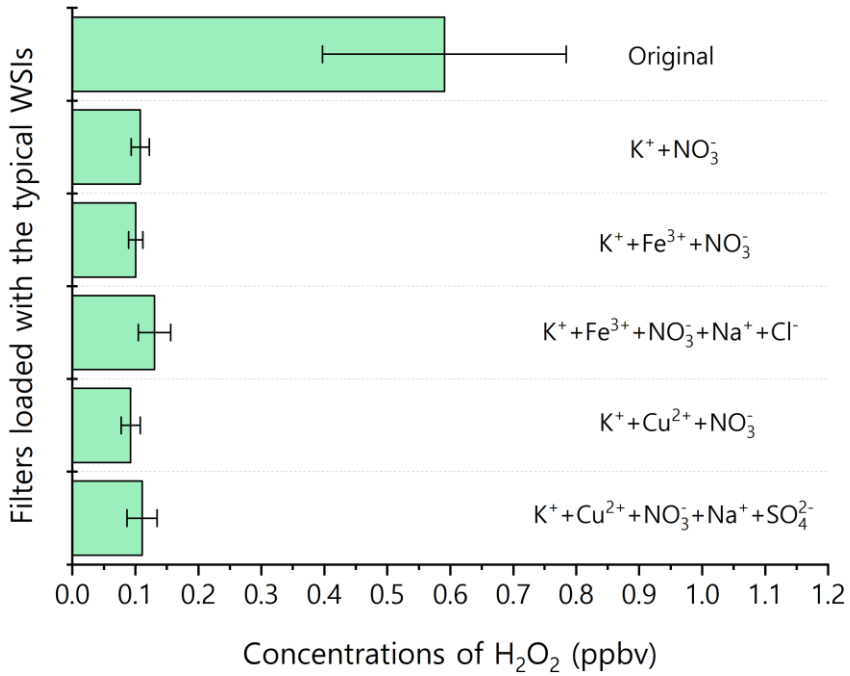

Fig. S7. The influence of typical water-soluble ions on H_2O_2 production from pre-treated filter samples under irradiation of the UV lamps in the flow tube. The experiments were carried out for blank filters loaded with $K^+ + NO_3^-$, $Fe^{3+} + K^+ + NO_3^-$, $Fe^{3+} + K^+ + NO_3^- + Na^+ + Cl^-$, $Cu^{2+} + K^+ + NO_3^-$ and $Cu^{2+} + K^+ + NO_3^- + Na^+ + SO_4^{2-}$ by flushing synthesis air with ~15% RH, respectively. The green bars represent the average concentration of H_2O_2 under 2h UV irradiation.

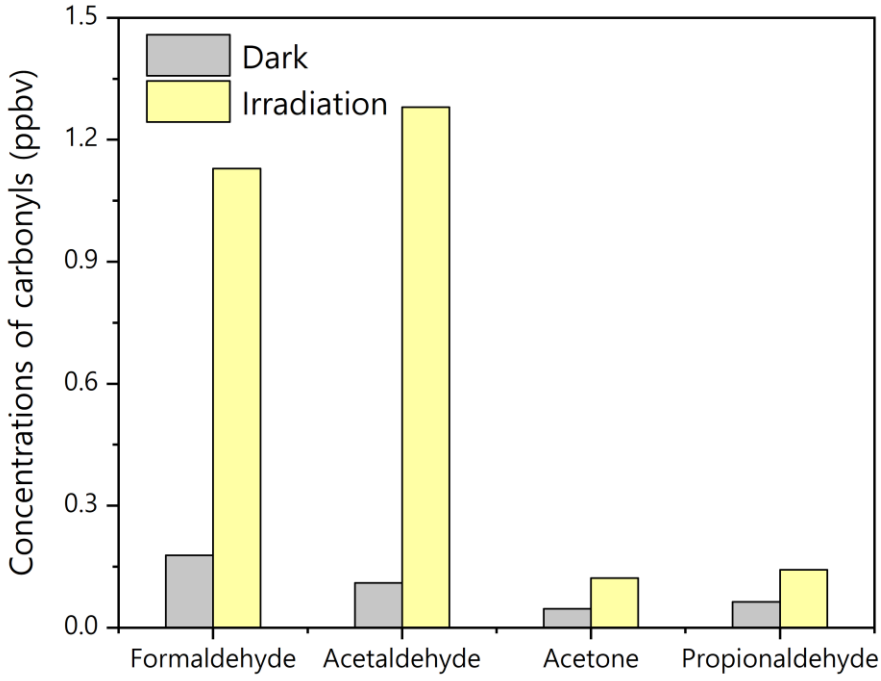

Fig. S8. The carbonyls (formaldehyde, acetaldehyde, acetone and propionaldehyde) production from $PM_{2.5}$ filter sample under irradiation of the UV lamps in the flow tube. The experiment was carried out for the $PM_{2.5}$ filter sample (WD-18-Jan-19) by flushing humidified synthesis air of ~15% RH (296 ± 2K) at a flow rate of 5L min^{-1} under 1h dark and 1h irradiation conditions.

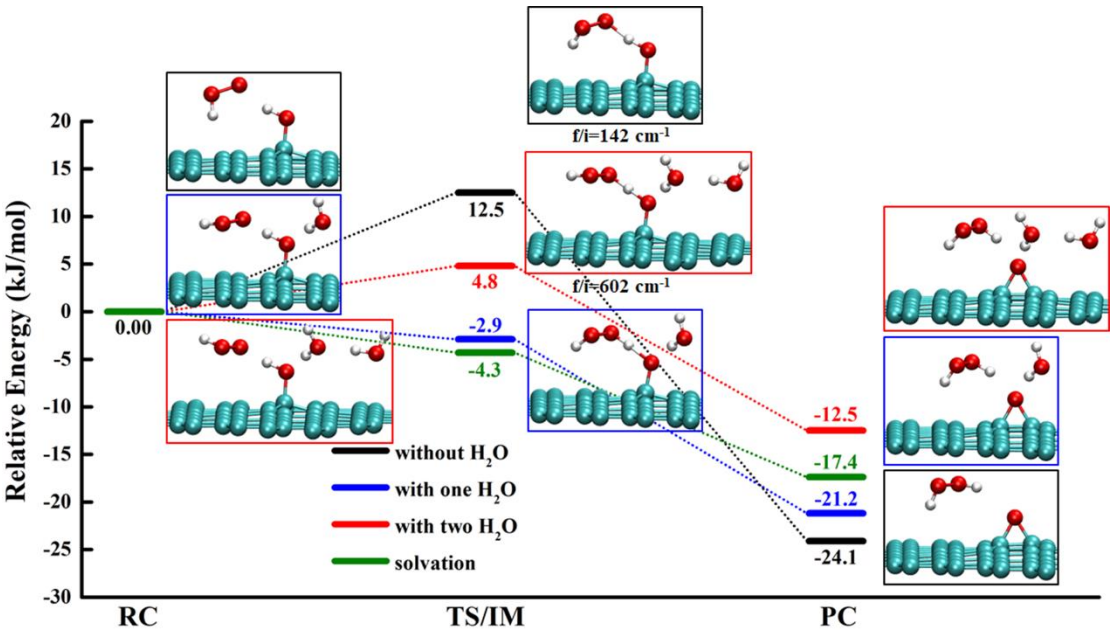

Fig. S9. Pathway for the reactions of HO_2 radicals with surface hydroxyl to produce H_2O_2 over carbonaceous soot surfaces with and without the presence of water molecules as well as the optimized geometries of the reactant complex (RC), transition states (TS), intermediate species (IM), and product complex (PC). Cyan, red, white, and yellow circles denote C, O, H, and S atoms, respectively. The imaginary frequency of the transition state is presented.

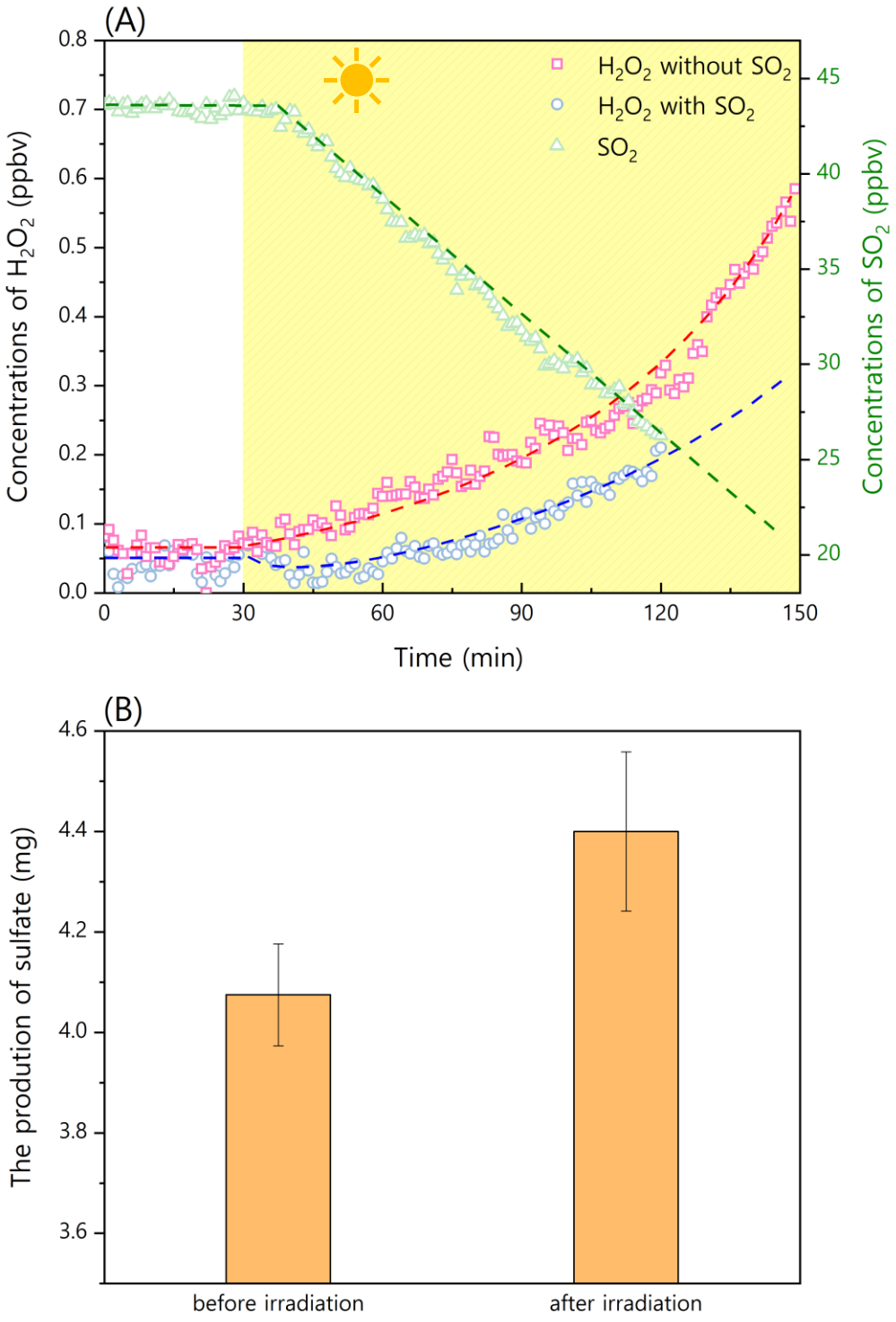

Fig. S10. The variations of H_2O_2 and SO_2 (A) and the production of sulfate (B) for $PM_{2.5}$ filter samples under irradiation of the UV lamps in the chamber. The experiments were carried out for three parallel $PM_{2.5}$ filter samples (WD-25-Dec-19) with and without the presence of SO_2 in humidified synthesis air of ~30% RH. The blank areas and the yellow shadows in (A) represent the dark condition and the UV irradiation, respectively.

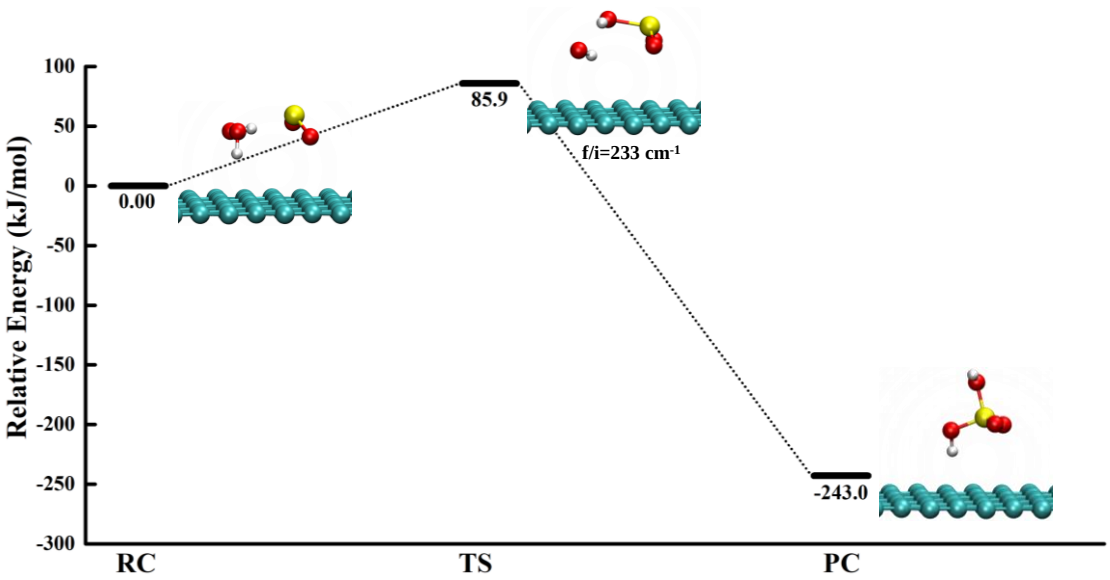

Fig. S11. Pathway for the reactions of SO_2 with H_2O_2 to produce H_2SO_4 over carbonaceous soot surfaces and the optimized geometries of the reactant complex (RC), transition states (TS), and product complex (PC). Cyan, red, white, and yellow circles denote C, O, H, and S atoms, respectively. The imaginary frequency of the transition state is presented.

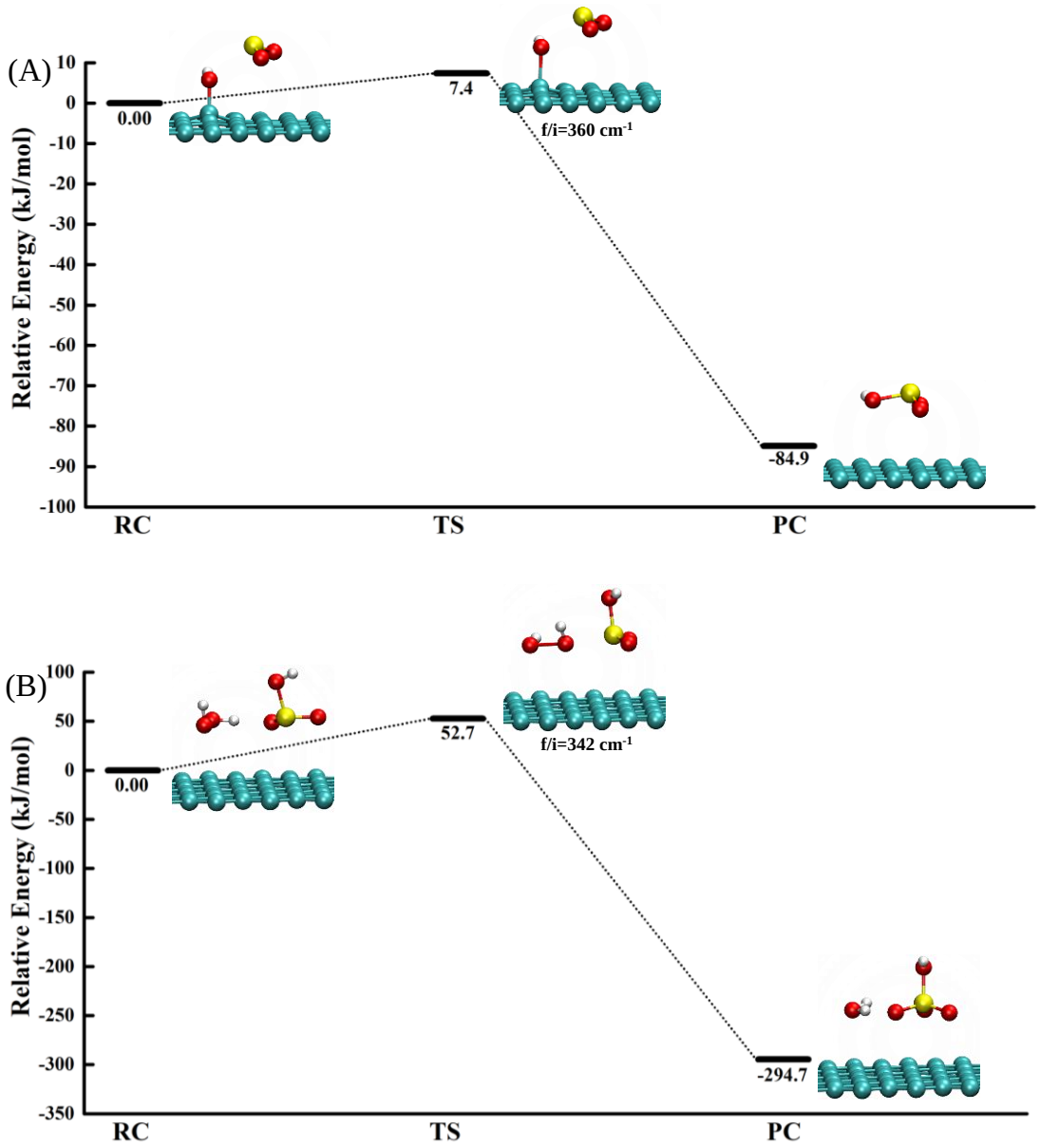

Fig. S12. Pathway for the oxidation of SO_2 by H_2O_2 with surface -OH assistance over carbonaceous soot surfaces and the optimized geometries of the reactant complex (RC), transition states (TS), and product complex (PC). (A) The reaction of SO_2 with surface -OH to produce $H_2SO_3^-$. **(B)** The reaction of $H_2SO_3^-$ with H_2O_2 to produce HSO_4^- and H_2O. Cyan, red, white, and yellow circles denote C, O, H, and S atoms, respectively. The imaginary frequency of the transition state is presented.

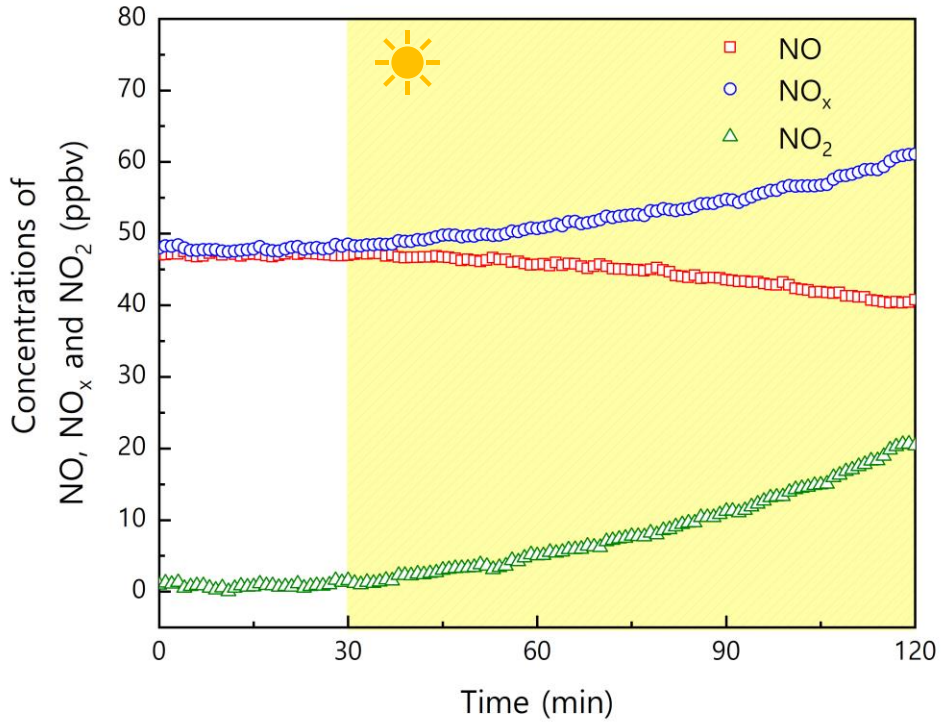

Fig. S13. The variations of NO, NO_2 and NO_x for $PM_{2.5}$ filter samples under irradiation of the UV lamps in the chamber. The experiment was carried out for three parallel $PM_{2.5}$ filter samples (WD-25-Dec-19) with and without the presence of NO in humidified synthesis air of ~30% RH. The blank areas and the yellow shadows represent the dark condition and the UV irradiation, respectively.

Table S1. The mass concentrations (μg m^{-3}) of WSIs, WSOC, MEs, OC, EC and $PM_{2.5}$ in the several typical $PM_{2.5}$ filter samples.

Species	BJ [a]	SH [a]	GZ [a]	Mel [a]	WD1 [b]	WD2 [b]	WD3 [b]
Na^+	4.75	1.03	0.92	0.18	1.54	4.19	10.52
Mg^{2+}	0.04	0.13	0.11	0.01	0.29	0.63	0.77
Ca^{2+}	0.34	0.64	0.98	0.04	1.79	3.26	2.41
K^+	1.24	0.67	0.69	0.09	1.79	4.07	3.01
NH_4^+	3.17	7.03	5.22	1.08	6.81	23.99	15.80
NO_3^-	7.01	26.32	11.32	2.55	12.80	46.44	19.25
SO_4^{2-}	6.66	7.48	12.70	0.96	7.57	17.47	16.66
Cl^-	4.53	1.04	0.50	0.10	7.68	25.86	11.25
WSOC	20.11	5.90	8.07	0.93	10.84	38.92	52.37
Al	2.32	0.55	0.58	0.10	0.88	3.69	1.75
Mn	0.78	0.04	0.05	0.01	0.07	0.15	0.25
Fe	4.79	0.44	0.53	0.13	1.09	1.44	1.88
Ni	0.57	0.00	0.01	0.00	0.03	0.07	0.20
Cu	0.42	0.02	0.02	0.00	0.04	0.44	0.26
Zn	0.00	0.00	0.14	0.01	0.38	0.28	1.29
As	0.91	0.02	0.02	0.01	0.04	0.11	0.21
Se	0.84	0.02	0.03	0.00	0.07	0.20	0.21
Ba	1.71	0.02	0.03	0.01	0.07	0.14	0.28
Pb	1.21	0.06	0.05	0.01	0.11	0.31	0.31
OC	63.30	8.71	11.02	1.36	22.16	99.23	126.84
EC	17.25	4.17	4.75	0.78	12.42	49.49	60.02
$PM_{2.5}$	146.27	62.44	54.83	7.96	88.15	334.18	342.63

[a] BJ: Beijing; SH: Shanghai; GZ: Guangzhou; Mel: Melpitz,

[b] WD1: WD-2-Jan-20; WD2: WD-18-Jan-19; WD3: WD-13-Dec-18

References

1. Liu, P.; Zhang, C.; Xue, C.; Mu, Y.; Liu, J.; Zhang, Y.; Tian, D.; Ye, C.; Zhang, H.; Guan, J., The contribution of residential coal combustion to atmospheric $PM_{2.5}$ in northern China during winter. *Atmospheric Chemistry and Physics* **2017,** *17*, (18), 11503-11520.

2. Xue, C.; Zhang, C.; Ye, C.; Liu, P.; Catoire, V.; Krysztofiak, G.; Chen, H.; Ren, Y.; Zhao, X.; Wang, J.; Zhang, F.; Zhang, C.; Zhang, J.; An, J.; Wang, T.; Chen, J.; Kleffmann, J.; Mellouki, A.; Mu, Y., HONO Budget and Its Role in Nitrate Formation in the Rural North China Plain. *Environ Sci Technol* **2020,** *54*, (18), 11048-11057.

3. Lazrus, A. L.; Kok, G. L.; Lind, J. A.; Gitlin, S. N.; Heikes, B. G.; Shetter, R. E., Automated fluorometric method for hydrogen peroxide in air. *Analytical Chemistry* **1986,** *58*, (3), 594-597.

4. Hecobian, A.; Zhang, X.; Zheng, M.; Frank, N.; Edgerton, E. S.; Weber, R. J., Water-Soluble Organic Aerosol material and the light-absorption characteristics of aqueous extracts measured over the Southeastern United States. *Atmospheric Chemistry and Physics* **2010,** *10*, (13), 5965-5977.

5. Cheng, Y.; He, K. B.; Zheng, M.; Duan, F. K.; Du, Z. Y.; Ma, Y. L.; Tan, J. H.; Yang, F. M.; Liu, J. M.; Zhang, X. L.; Weber, R. J.; Bergin, M. H.; Russell, A. G., Mass absorption efficiency of elemental carbon and water-soluble organic carbon in Beijing, China. *Atmospheric Chemistry and Physics* **2011,** *11*, (22), 11497-11510.

6. Wu, G.; Wan, X.; Gao, S.; Fu, P.; Yin, Y.; Li, G.; Zhang, G.; Kang, S.; Ram, K.; Cong, Z., Humic-Like Substances (HULIS) in Aerosols of Central Tibetan Plateau

(Nam Co, 4730 m asl): Abundance, Light Absorption Properties, and Sources. *Environ Sci Technol* **2018,** *52*, (13), 7203-7211.

7. Liu, P.; Ye, C.; Xue, C.; Zhang, C.; Mu, Y.; Sun, X., Formation mechanisms of atmospheric nitrate and sulfate during the winter haze pollution periods in Beijing: gas-phase, heterogeneous and aqueous-phase chemistry. *Atmospheric Chemistry and Physics* **2020,** *20*, (7), 4153-4165.

8. Liu, P.; Zhang, C.; Mu, Y.; Liu, C.; Xue, C.; Ye, C.; Liu, J.; Zhang, Y.; Zhang, H., The possible contribution of the periodic emissions from farmers' activities in the North China Plain to atmospheric water-soluble ions in Beijing. *Atmospheric Chemistry and Physics* **2016,** *16*, (15), 10097-10109.

9. Li, X.; Zhang, C.; Liu, P.; Liu, J.; Zhang, Y.; Liu, C.; Mu, Y., Significant influence of the intensive agricultural activities on atmospheric $PM_{2.5}$ during autumn harvest seasons in a rural area of the North China Plain. *Atmospheric Environment* **2020,** *241*, 117844.

10. Ma, Z.; Liu, C.; Zhang, C.; Liu, P.; Ye, C.; Xue, C.; Zhao, D.; Sun, J.; Du, Y.; Chai, F.; Mu, Y., The levels, sources and reactivity of volatile organic compounds in a typical urban area of Northeast China. *J Environ Sci (China)* **2019,** *79*, 121-134.

11. Wang, J.; Sun, S.; Zhang, C.; Xue, C.; Liu, P.; Zhang, C.; Mu, Y.; Wu, H.; Wang, D.; Chen, H.; Chen, J., The pollution levels, variation characteristics, sources and implications of atmospheric carbonyls in a typical rural area of North China Plain during winter. *J Environ Sci (China)* **2020,** *95*, 256-265.

12. Pang, X. B.; Mu, Y. J., Seasonal and diurnal variations of carbonyl compounds in Beijing ambient air. *Atmospheric Environment* **2006,** *40*, (33), 6313-6320.

13. Zhang, Y. J.; Mu, Y. J.; Liu, J. F.; Mellouki, A., Levels, sources and health risks of carbonyls and BTEX in the ambient air of Beijing, China. *Journal of Environmental Sciences* **2012,** *24*, (1), 124-130.

14. Perdew, J. P.; Burke, K.; Ernzerhof, M., Generalized gradient approximation made simple. *Phys. Rev. Lett.* **1996,** *77*, (18), 3865-3868.

15. Kresse, G.; Furthmuller, J., Efficient iterative schemes for ab initio total-energy calculations using a plane-wave basis set. *Phys. Rev. B* **1996,** *54*, (16), 11169-11186.

16. Kresse, G.; Joubert, D., From ultrasoft pseudopotentials to the projector augmented-wave method. *Phys. Rev. B* **1999,** *59*, (3), 1758-1775.

17. He, G.; Ma, J.; He, H., Role of Carbonaceous Aerosols in Catalyzing Sulfate Formation. *ACS Catalysis* **2018,** *8*, (5), 3825-3832.

18. He, G.; He, H., Water Promotes the Oxidation of SO_2 by O_2 over Carbonaceous Aerosols. *Environ Sci Technol* **2020,** *54*, (12), 7070-7077.

19. Henkelman, G.; Jonsson, H., Improved tangent estimate in the nudged elastic band method for finding minimum energy paths and saddle points. *J. Chem. Phys.* **2000,** *113*, (22), 9978-9985.

20. Henkelman, G.; Uberuaga, B. P.; Jonsson, H., A climbing image nudged elastic band method for finding saddle points and minimum energy paths. *J. Chem. Phys.* **2000,** *113*, (22), 9901-9904.

21. He, G. Z.; Lian, Z. H.; Yu, Y. B.; Yang, Y.; Liu, K.; Shi, X. Y.; Yan, Z. D.; Shan, W. P.; He, H., Polymeric vanadyl species determine the low-temperature activity of V-based catalysts for the SCR of NO_x with NH_3. *Science Advances* **2018,** *4*, eaau4637.